Electrification in turbulent channel flows of liquid dielectrics

Mathieu Calero,[1, a)] Holger Grosshans,[2, b)] and Miltiadis V. Papalexandris[3, c)]
[1)] *Université catholique de Louvain, Institute of Mechanics, Materials and Civil Engineering, 1348 Louvain-la-Neuve, Belgium*
[2)] *Physikalisch-Technische Bundesanstalt (PTB), Division of Chemical Physics and Explosion Protection, 38116 Braunschweig, Germany*
[3)] *Université catholique de Louvain, Institute of Mechanics, Materials and Civil Engineering, 1348 Louvain-la-Neuve, Belgium*

Electrification of wall-bounded flows of liquid dielectrics occurs via transport of electric-charge carriers (ions) from the electrical double layer at a liquid-solid interface to the bulk of the flow. This phenomenon is currently not well understood but it has been proposed that flow turbulence plays a major role on it. However, conclusive studies about the role of turbulence and the underpinning mechanisms of flow electrification are still lacking. In this paper we report on Direct Numerical Simulations (DNS) of electrification in turbulent channel flow of liquid dielectrics and for friction Reynolds numbers ranging from 150 to 210. Our simulations confirm that turbulence increases dramatically the amount of charge transported in the bulk of the flow. Also, the electrification rate increases with the turbulence intensity. Nonetheless, ionic diffusion does not influence the electrification process, due to the large value of the ionic Schmidt number. Our simulations further predict that, upon electrification, the charge density profile consists of three zones. In the first one, adjacent to the wall, the dominant mechanism is ionic diffusion. Whereas in the second one the dominant mechanisms are convective and conductive currents. In the third zone, the bulk of the flow, the charge density remains almost constant. Also, according to the budget of the charge-density variance, molecular transport counterbalances molecular dissipation in the first zone, and production counterbalances turbulent transport in the second one. Finally, we provide a closed-form expression for the mean charge-density profile based on the gradient assumption which agrees well with our DNS results.

I. INTRODUCTION

This paper focuses on the electrification of flow of liquid dielectrics. Typically, this phenomenon occurs via transport of electric-charge carriers (ions) from liquid-solid interfaces to the bulk of the flow. However, the underpinning physical mechanisms are currently not well understood. On the other hand, it has long been established that physicochemical processes at a liquid-solid interface result in the formation of the electric double layer[1] (EDL), for which extensive studies were conducted. As shown by Stern[2], the EDL consists of two parallel charge layers. The first layer, located in the side of the solid, is called the surface charge. The second layer is in the liquid side and consists of two sublayers, namely, the Stern or compact layer and the diffuse layer. The Stern layer is so close to the wall that its electrical charge is independent of the fluid flow. Moreover, its charge has the opposite sign to that of the surface charge. The thickness of the Stern layer is at the order of the size of the charged particles (ions). The diffuse layer is characterized by a steep gradient of the charge concentration, which decreases away from the solid surface. In general, the thickness of the diffuse layer is quite small and at the order of the Debye length. Generally speaking, the Debye length is the characteristic length-scale of electrostatic effects in fluids and plasmas, and its value depends on the electrical properties of the medium[1]. The definition of the Debye length is provided in equation (18) below.

Flow electrification takes place when electric charges are transported away from the diffuse layer and towards the bulk of the flow. Typically, this phenomenon can occur in low-conductivity liquids; examples of such liquids are certain hydrocarbons such as toluene and benzene. The build-up of charge in liquids constitutes a safety hazard in the industrial and technological sectors because it can lead to electric discharges. In fact, over the years, flow electrification during the transport of liquid hydrocarbons has resulted in several major accidents; see for example the early report of Klinkenberg and van der Minne[3] and the more recent analysis of Ohsawa[4]. These accidents have spurred several authors to investigate this phenomenon in order to develop techniques to prevent its occurrence.

For instance, Touchard[5] first determined the space charge for a fluid at rest inside a pipe. More specifically, he provided an analytical expression in terms of modified Bessel functions under the assumption that the difference between anion and cation concentrations near the liquid-solid interface is much smaller than their sum. This is often referred to as the “weak space-charge density assumption" and is deemed to be valid for low-conductivity liquids such as liquid hydrocarbons. In the same paper, Touchard[5] also studied electrification of laminar flow in a pipe. Therein he reported that a laminar flow does not modify the space-charge density, resulting in a profile similar to that in a liquid at rest. Subsequently, this study was extended to wall-bounded laminar flows in simple cross-sectional geometries (channel, square duct, circular pipe, etc.) under the weak space-charge density assumption[6–9].

It has been proposed that flow turbulence plays a major role on electrification and can increase the amount of charge in the bulk[5,10]. However, the number of studies devoted to this topic is quite small. In such a study, based on experimental data, Touchard[5] proposed a charge-density profile in channel flows

[a)] Electronic mail: mathieu.calero@uclouvain.be
[b)] Electronic mail: holger.grosshans@ptb.de
[c)] Corresponding author: miltos@uclouvain.be

consisting of two delimited zones. According to it, the profile in the near-wall zone is the same as that in a liquid at rest. Whereas in the second zone, electrification is affected by turbulence and the space-charge density is uniform. This model however involves a discontinuity in the charge-density profile between the two zones. (Henceforth, for the sake of simplicity, the space-charge density, *i.e.* the charge density in the fluid, will be referred to as "charge density".) Subsequently, Cabaleiro *et al.* [11] presented a new model which yields continuous charge-density profiles by introducing a turbulent (eddy) diffusivity related to the convective current. These models have been recently reviewed by Touchard [12] and compared against experimental data by Touchard [13]. Also Clermont *et al.* [14,15] proposed models and performed experiments for conductive currents in circular pipes.

Abedian and Sonin [16] also studied turbulent flow electrification in circular pipes. More specifically, they derived a close-form expression for the mean charge-density profile (in the radial direction) for fully developed flow by employing the gradient assumption for the unresolved turbulent fluxes of the electric charge. In a subsequent paper, Abedian and Sonin [17] showed that this expression compares favourably with available experimental data, including those of Hampel and Luther [18] for materials with large Debye lengths. Modeling approaches and numerical results relying on the eddy-viscosity concept have recently been presented by Ratschow, Stein, and Gross [19] and Diao *et al.* [20].

However, those earlier works examined the charge-density profiles in flows that had already been electrified, without focusing on the electrification process and its underpinning mechanisms. To our knowledge, conclusive studies about the role of turbulence and the mechanisms of turbulent flow electrification are still lacking. This paper aims to fill this gap by presenting Direct Numerical Simulations (DNS) of electric charge transport in turbulent channel flows of liquid dielectrics. The main objectives of the present study are to provide insight into the process of flow electrification, describe the various stages of this phenomenon, and analyze the statistical properties of the charge density.

In the recent past, advancements in algorithm development have enabled the numerical study of a variety of problems arising in electrohydrodynamics. Essentially, these algorithms consist of two coupled components, namely, one solver for the fluid-flow equations (typically the Navier-Stokes equations) and another one governing equations of electrostatics; see, for example, López-Herrera, Popinet, and Herrada [21], Roghair, van den Ende, and Mugele [22], Calero, Grosshans, and Papalexandris [23] and references therein. In our simulations, we have made use of pafiX [24] which is a computational tool that we developed for the simulation of powder and fluid-flow operations in process industries with an emphasis on phenomena that represent a hazard to operational safety. This computational tool is available as freeware.

The paper is structured as follows. In section II we present the governing equations of the problem in hand. In section III we examine two special cases so as to highlight the role of each term in the charge-density equation to the electrification process. In section IV we outline the numerical setup. Subsequently, in section V we present and analyze the numerical results. Finally, section VI concludes.

II. GOVERNING EQUATIONS

In this section, we describe the system of governing equations of electrohydrodynamics for incompressible flows of liquid dielectrics. This system consists of three coupled parts, namely the Navier-Stokes equations (supplemented with the Lorentz force), Gauss' law for the electric field and the conservation equation of the electric charge. The fluid density and temperature are assumed to be constant. The mass and momentum balance laws for the flows of interest, read,

$$\nabla \cdot \boldsymbol{u} = 0, \tag{1}$$

$$\frac{\partial \boldsymbol{u}}{\partial t} + (\boldsymbol{u} \cdot \nabla)\boldsymbol{u} = -\frac{1}{\rho}\nabla p + \nu \nabla^2 \boldsymbol{u} + \frac{1}{\rho}\boldsymbol{F}_{\mathrm{el}}, \tag{2}$$

where $\boldsymbol{u} = (u, v, w)$ is the velocity vector, ρ the mass density, p the dynamic pressure and ν the kinematic viscosity of the fluid. Further, $\boldsymbol{F}_{\mathrm{el}}$ stands for the Lorentz force, *i.e.* the volumetric electric force acting on the fluid, and can be derived from the electrostatic Maxwell stress tensor[25]. For non-polar media, it is equal to the product between the electric field $\boldsymbol{E}$ and the charge density ρ_{el},

$$\boldsymbol{F}_{\mathrm{el}} = \rho_{\mathrm{el}}\, \boldsymbol{E}. \tag{3}$$

In the applications of interest, dynamic currents due to charge transport are very small so that the effects of electromagnetic induction are negligible[26]. Accordingly, the laws of electrodynamics are simplified to those of electrostatics. In particular, the electric field $\boldsymbol{E}$ satisfies Gauss' law,

$$\nabla \cdot \boldsymbol{E} = \frac{\rho_{\mathrm{el}}}{\epsilon}, \tag{4}$$

where ρ_{el} is the electric charge density and ϵ is the homogeneous electrical permittivity. Also, since in the electrostatic approximation the electric field is irrotational, it can be written in terms of the gradient of the electric potential ϕ,

$$\boldsymbol{E} = -\nabla \phi. \tag{5}$$

Accordingly, Gauss' law reduces to the following Poisson equation,

$$\nabla^2 \phi = -\frac{\rho_{\mathrm{el}}}{\epsilon}. \tag{6}$$

As already mentioned above, this paper focuses on liquid dielectrics. These materials are characterized by absence of loosely bound or free electrons that can move from one molecule to another. In such materials, however, there are impurities which dissociate and their ions participate in the electrochemical reactions that take place at the liquid solid-wall interface leading to the formation of the EDL. Further, at typical impurity concentrations, conductivity is caused by these ions because electrons are trapped by the neutral electron-acceptor molecules[27]. Accordingly, only ionic carriers need

to be taken into account and the free-electron concentration can be neglected[26,27]. The charge density ρ_{el}, for the flows of interest is then given by[28],

$$\rho_{\mathrm{el}} \;=\; \sum_{\mathrm{P}} e_0 z_{\mathrm{P}} n_{\mathrm{P}} - \sum_{\mathrm{N}} e_0 z_{\mathrm{N}} n_{\mathrm{N}}\,, \tag{7}$$

where n_{P} and n_{N} are, respectively, the concentrations of cations and anions in the liquid and e_0 is the elementary charge. Further, z_{P} and z_{N} denote, respectively, the absolute values of the valences of cations and anions. Also, the electric conductivity is defined as[28],

$$\sigma \;=\; \frac{e_0^2}{K_{\mathrm{B}} T}\left(D_{\mathrm{P}} z_{\mathrm{P}}^2 n_{\mathrm{P}} + D_{\mathrm{N}} z_{\mathrm{N}}^2 n_{\mathrm{N}}\right), \tag{8}$$

where D_{P} and D_{N} are, respectively, the diffusion coefficients of cations and anions in the liquid. Further, K_{B} represents the Boltzmann constant, while T is the temperature of the liquid (assumed to be constant).

The specific electric current densities for cations and anions are given by[28],

$$\boldsymbol{J}_{\mathrm{P}} \;=\; -e_0 z_{\mathrm{P}} D_{\mathrm{P}} \nabla n_{\mathrm{P}} + \frac{e_0^2 z_{\mathrm{P}}^2 D_{\mathrm{P}} n_{\mathrm{P}}}{K_{\mathrm{B}} T}\boldsymbol{E} + e_0 z_{\mathrm{P}} n_{\mathrm{P}} \boldsymbol{u}\,, \tag{9}$$

$$\boldsymbol{J}_{\mathrm{N}} \;=\; e_0 z_{\mathrm{N}} D_{\mathrm{N}} \nabla n_{\mathrm{N}} + \frac{e_0^2 z_{\mathrm{N}}^2 D_{\mathrm{N}} n_{\mathrm{N}}}{K_{\mathrm{B}} T}\boldsymbol{E} - e_0 z_{\mathrm{N}} n_{\mathrm{N}} \boldsymbol{u}\,, \tag{10}$$

In each of equations (9) and (10), the first term on the right-hand side represents ionic diffusion, the second term represents ionic migration, and the third one describes ionic convection. Additionally, the total electric current density, $\boldsymbol{J}$, is defined as the sum of the specific current densities for cations and anions, namely,

$$\boldsymbol{J} \;=\; \sum_{\mathrm{P}} \boldsymbol{J}_{\mathrm{P}} + \sum_{\mathrm{N}} \boldsymbol{J}_{\mathrm{N}}\,. \tag{11}$$

Accordingly, the conservation equation for the electric charge density reads,

$$\frac{\partial \rho_{\mathrm{el}}}{\partial t} + \nabla \cdot \boldsymbol{J} \;=\; 0\,. \tag{12}$$

In order to simplify the expression for $\boldsymbol{J}$, hence for (12), we introduce herein the following assumptions:

i The ionic valences are all equal to a specific value, often unity, denoted by z,

$$z_{\mathrm{P}} \;=\; z_{\mathrm{N}} \;=\; z\,. \tag{13}$$

ii. The diffusion coefficients of all ionic species are equal, denoted by D,

$$D_{\mathrm{P}} \;=\; D_{\mathrm{N}} \;=\; D\,. \tag{14}$$

iii. The sum of the concentrations of cations and anions is much higher than their difference,

$$\sum_{\mathrm{P}} n_{\mathrm{P}} + \sum_{\mathrm{N}} n_{\mathrm{N}} \;\gg\; \sum_{\mathrm{P}} n_{\mathrm{P}} - \sum_{\mathrm{N}} n_{\mathrm{N}}\,. \tag{15}$$

These assumptions are commonly employed in the study of flows in the presence of electrostatic fields[5,16,29] and are deemed to be valid for the fluids of interest, *i.e.* liquid dielectrics.

By virtue of these three assumptions, the electric conductivity σ becomes independent of the electric charge density. In particular, the expression (8) of σ reduces to,

$$\sigma \;=\; \frac{e_0^2\, D\, n_0}{K_{\mathrm{B}} T}\,, \tag{16}$$

with n_0 being the total ionic concentration in the liquid, $n_0 = \sum_{\mathrm{P}} n_{\mathrm{P}} + \sum_{\mathrm{N}} n_{\mathrm{N}}$.

Additionally, by introducing (9) and (10) into (11) and by making use of (13), (14), and (16), we readily obtain the following expression for the total current density[28],

$$\boldsymbol{J} \;=\; -D\nabla\rho_{\mathrm{el}} + \sigma\boldsymbol{E} + \rho_{\mathrm{el}}\boldsymbol{u}\,, \tag{17}$$

This expression can then be directly substituted in (12). In other words, the aforementioned assumptions, (13)-(15) allow for the introduction of a single conservation equation for the charge density (global analysis) instead of the use of a conservation equation for each ionic species (local analysis)[26].

One important benefit stemming from this simplification is that it is no longer required to determine the rates of chemical reactions such as recombination and production of cations or anions. This feature is particularly important in the case of liquid hydrocarbons, because such reaction rates are not readily available for them. As a matter of fact, in the electrification of these substances, the dominant ionized species are typically unknown impurities[16].

The definition of the Debye length is given by[8],

$$\lambda_{\mathrm{D}} \;=\; \sqrt{\frac{\epsilon\, K_{\mathrm{B}} T}{e_0^2\, n_0}}\,. \tag{18}$$

Then, in view of the definition (16) of the electrical conductivity, the Debye length is also written as,

$$\lambda_{\mathrm{D}} \;=\; \sqrt{\frac{\epsilon\, D}{\sigma}}\,. \tag{19}$$

By employing the continuity equation (1), Gauss' law (4) and the expression (17) for $\boldsymbol{J}$, the balance law of the electric charge in (12) is written as follows,

$$\frac{\partial \rho_{\mathrm{el}}}{\partial t} + \boldsymbol{u}\cdot\nabla\rho_{\mathrm{el}} \;=\; -\frac{\sigma}{\epsilon}\rho_{\mathrm{el}} + \boldsymbol{E}\cdot\nabla\sigma + \nabla\cdot\left(D\nabla\rho_{\mathrm{el}}\right). \tag{20}$$

The diffusivity D is a function of the temperature and the ion mobility which in turn depends on the fluid density. Since both the temperature and the fluid density are constant, then D is taken to be constant too.

Further, the electric conductance of a liquid dielectric is due to impurities only which carry ions. The concentration of the impurities is very small and cannot be known precisely. Nonetheless, it is reasonable to assume that it remains nearly

constant in the flow domain; this has been a common assumption in previous studies on liquid dielectrics[6,30]. Therefore, the total ionic concentration n_0 can also be approximated as constant. According to Touchard et al.[6], this is also inferred from the hypothesis (15) that the difference between anion and cation concentrations is much smaller than their sum n_0. Consequently, in view of (16), the conductivity σ can be approximated to be constant as well. This approximation is also made by necessity due to the scarcity of data for σ at different concentrations of impurities in liquid dielectrics. Then, with these approximations, the above balance law of ρ_{el} is reduced to,

$$\frac{\partial \rho_{\mathrm{el}}}{\partial t} + \boldsymbol{u} \cdot \nabla \rho_{\mathrm{el}} \;=\; -\frac{\sigma}{\epsilon}\rho_{\mathrm{el}} + D\nabla^2 \rho_{\mathrm{el}}\,. \tag{21}$$

This is an advection-diffusion-reaction equation. The second term on the left-hand side of this equation describes convection of charge, *i.e.* the convective currents. The first term on the right-hand side of (21) describes the conductive currents (*i.e.* ohmic resistance) and acts as a counterweight to charge accumulation, while the second term describes diffusion of charge. Due to the conductive current, the behaviour of the charge density ρ_{el} is quite different from that of a passively advected scalar.

With regard to electrification in turbulent channel flows, the important dimensionless group of the hydrodynamic component of the governing equations is the Reynolds number. Herein we make use of the friction Reynolds number $Re_\tau = u_\tau h/\nu$, where h is the half-width of the channel and u_τ is the friction velocity; $u_\tau = \sqrt{\tau_{\mathrm{w}}/\rho}$ with τ_{w} being the wall shear stress. Also, in *dimensionless* form, the conservation equation for the charge (21) becomes,

$$\frac{\partial \rho_{\mathrm{el}}}{\partial t} + \boldsymbol{u} \cdot \nabla \rho_{\mathrm{el}} \;=\; -r_t \rho_{\mathrm{el}} + \frac{1}{Re_\tau\, Sc}\nabla^2 \rho_{\mathrm{el}}\,, \tag{22}$$

where r_t is the ratio between the hydrodynamic and electrostatic time scales and Sc is the Schmidt number related to the ionic diffusivity,

$$r_{\mathrm{t}} \;=\; \frac{h/u_\tau}{\epsilon/\sigma}\,, \qquad\qquad Sc \;=\; \frac{\nu}{D}\,. \tag{23}$$

As a matter of fact, the ratio ϵ/σ is known as the electric relaxation time[21]. Another relevant group is the ratio between the Debye length and the length scale of the domain (which in our case is the channel half-width h),

$$r_{\mathrm{l}} \;=\; \frac{\lambda_{\mathrm{D}}}{h}\,. \tag{24}$$

In fact, the following relation holds, $Re_\tau\, Sc = 1/(r_{\mathrm{t}} r_{\mathrm{l}}{}^2)$. Herein, for the purpose of simplicity of notation we will not use different symbols for dimensionless quantities because it is straightforward to determine if a given variable is provided in dimensional or dimensionless form without loss of clarity.

III. SPECIAL CASES

In order to provide some insight about the electrification process in channel flows and to highlight the role of the various terms in the charge-density equation (21), we analyze below two special cases, namely, flow with no charge diffusion and laminar flow. In these two special cases, we assume that the Lorentz force is negligibly small, so that the Navier-Stokes and electrostatics equations essentially decouple. Henceforth, x will denote the streamwise coordinate of the channel, while y and z will denote the normal and spanwise directions respectively.

i) *No ionic diffusion*

In some studies, the diffusion term is neglected, especially when the Debye length is several order of magnitudes smaller than the reference length of the flow domain[21]. Without the diffusion term, the charge balance law (21) reads,

$$\frac{\partial \rho_{\mathrm{el}}}{\partial t} + \boldsymbol{u} \cdot \boldsymbol{\nabla} \rho_{\mathrm{el}} \;=\; -\frac{\sigma}{\epsilon}\rho_{\mathrm{el}}\,. \tag{25}$$

Let $s \mapsto \boldsymbol{X}(s,t,\boldsymbol{x})$ be the characteristic curve defined, for $0 < s < t$, by,

$$\begin{cases} \dfrac{\mathrm{d}}{\mathrm{d}s}\boldsymbol{X}(s,t,\boldsymbol{x}) \;=\; \boldsymbol{u}\left(s, \boldsymbol{X}(s,t,\boldsymbol{x})\right)\,, \\[2ex] \quad \boldsymbol{X}(t,t,\boldsymbol{x}) \;=\; \boldsymbol{x}. \end{cases} \tag{26}$$

By applying the method of characteristics in (25), we obtain,

$$\rho_{\mathrm{el}}(t,\boldsymbol{x}) \;=\; \rho_{\mathrm{el}}\left(\boldsymbol{X}(0,t,\boldsymbol{x})\right) \;\exp\left(-\frac{\sigma}{\epsilon}t\right). \tag{27}$$

According to this solution, there is no transport of charge away from solid-liquid interfaces, *i.e.* in the cross-stream direction. Instead, the initial charge decays exponentially with time along streamlines. This in turn implies that even though the diffusive term has a negligible effect in the bulk of the flow, it is still very important in the overall electrification process because it controls the diffusion of charge off the wall and the formation of the diffuse layer of the EDL. In particular, without this term, there would be no diffuse layer hence no electrification.

Evidently, the use of the method of characteristics for the charge-density equation presumes a given velocity field. Further, the domain of definition of the solution obtained in (27) depends strongly on the velocity $\boldsymbol{u}$. Accordingly, this method can only be applied in the special cases where the velocity distribution is known.

ii) *Laminar flow*

In laminar flows in ducts or pipes, and assuming that the Lorentz force is negligible, the velocity vector is normal to the charge-density gradient, which means that the convective current vanishes. Then, equation (21) reduces to,

$$\frac{\partial \rho_{\mathrm{el}}}{\partial t} \;=\; -\frac{\sigma}{\epsilon}\rho_{\mathrm{el}} + D\nabla^2 \rho_{\mathrm{el}}\,. \tag{28}$$

This equation can be solved numerically with a variety of algorithms. Also, analytical or semi-analytical solutions can be obtained for simple geometries. The steady-state version of (28) is the modified Helmholtz equation, the solution of which can readily be computed.

For the special but important case of laminar channel flow with prescribed charge densities at the walls, the steady-state

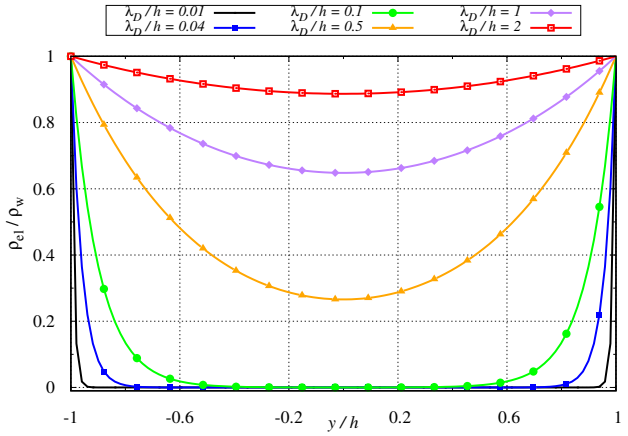

FIG. 1. Steady-state profiles of the charge-density distribution in laminar channel flow.

solution of (28) can be obtained in closed form. In order to fix ideas, let us consider a channel whose walls are located at $y = -h$ and $y = h$, respectively. Also, let ρ_a and ρ_b be the values for the charge at the two walls according to the prescribed Dirichlet condition. Then, the steady-state solution of (28) is given by,

$$\lim_{t\to+\infty} \rho_{\rm el}\,(y) \;=\; \frac{\rho_a \sinh\left(\frac{h-y}{\lambda_{\rm D}}\right) + \rho_b \sinh\left(\frac{h+y}{\lambda_{\rm D}}\right)}{\sinh\left(\frac{2h}{\lambda_{\rm D}}\right)}, \qquad (29)$$

Since in laminar channel flow $\boldsymbol{u}\cdot\nabla\rho_{\rm el} = 0$, then (29) is also the expression for the charge-density profile in the diffuse layer, *i.e.* if the fluid was at rest. According to this solution, the diffusion of charge in the bulk of the flow is counteracted by the ohmic conduction. The parameter that controls this process is the Debye length $\lambda_{\rm D}$ defined by (19). More specifically, the electrification of the fluid in the bulk increases greatly with $\lambda_{\rm D}$.

In many applications in the industrial and technological sectors, the Debye length is much smaller than the channel width $2h$, which explains why flow electrification very rarely occurs in laminar flows. Nonetheless, according to the solution (29), flow electrification is possible even in laminar flows for sufficiently narrow channels. In figure 1 we present plots of the steady-state profiles of $\rho_{\rm el}$ when $\rho_a = \rho_b$ and for various Debye lengths $\lambda_{\rm D}$. From these plots, we readily confirm that the electrification of the fluid increases strongly when Debye length $\lambda_{\rm D}$ (or, equivalently, r_l) increases.

IV. NUMERICAL SETUP

The governing system (1), (2), (6) and (21) is integrated numerically via the algorithm proposed by Calero, Grosshans, and Papalexandris [23]. It consists of a SIMPLE-based Navier-Stokes solver for (1) and (2)[31], coupled with a Poisson solver based on Jacobi iterations for the Poisson equation (6) of the electric potential and an upwind method for the charge-density equation (21). This algorithm has been parallelized using the Message Passing Interface (MPI) protocol and implemented in a Cartesian mesh with a staggered-grid arrangement. As mentioned in the introduction, it is part of the computational tool pafiX [24] for electrohydrodynamics simulations. The Navier-Stokes and Poisson solvers have already used in simulations of flows with charged particles[32–34]. Validation tests for the combined algorithm have been presented by Calero, Grosshans, and Papalexandris [23].

Symbol	Quantity	Value
ρ	Mass density[36]	879 Kg/m^3
ν	Kinematic viscosity[37]	7.24×10^{-7} m^2/s
ϵ	Permittivity[38]	2.01×10^{-11} F/m
σ	Conductivity[39]	1.1×10^{-12} S/m
D	Diffusion coefficient[40]	2.21×10^{-11} m^2/s

TABLE I. Material properties of benzene at room temperature.

The computational domain consists of a channel that is periodic in the streamwise and spanwise directions, x and z directions respectively. The half-width of the channel is denoted by h and its midplane is assumed to be located at $y = 0$. The length of the channel is $4\pi h$ (streamwise direction x), its width is $2h$ (direction y), and its depth $4\pi h/3$ (spanwise direction z). The numerical setup is similar to that of Kim, Moin, and Moser [35] for direct numerical simulations of channel flow at moderate turbulence intensities. The half-width of the channel is set at $h = 0.5$ cm.

Also, the working liquid is benzene, the properties of which at room temperature are listed in table I. In relation to flow electrification, its electrical conductivity σ is particularly low, as is the case for several liquid hydrocarbons. Given the above parameters, the Debye length of benzene is $\lambda_{\rm D} \approx 2.04\times10^{-5}$ m.

Herein we present simulations of five cases using three different flow rates (*i.e.* three different values of Re_τ) and three different sets of material parameters D and ϵ/σ (corresponding to two different values of the Debye length). In all cases, the Debye length is taken sufficiently small so that flow electrification does take place. The values of the material properties and flow parameters for each case are provided in table II. In this table, the friction Reynolds number Re_τ and the turbulent kinetic energy at the midplane k serve as measures of the turbulence intensity of the flow field. For completion purposes, the precise definition of k is provided in equation (31) below. Additionally, the values of the relevant dimensionless groups (Re_τ, $r_{\rm t}$, Sc) along with the value of the length-scale ratio $r_{\rm l}$ are given in table III.

In order to accelerate the electrification process, in cases A, B and C we have increased the value of the diffusion coefficient D, with respect to the actual value for benzene by approximately 50%. Additionally, in cases D and E, we have modified the values of ϵ/σ and D, respectively, in order to assess their effect on the overall process of flow electrification. In terms of relevant dimensionless groups, comparisons between cases A, B and C concern the effect of Re_τ. Comparisons between cases C and D are made so as to explore the role of the time-scale ratio $r_{\rm t}$, while comparisons between cases C

and E help assess the role of the ionic Schmidt number Sc. Since the present study consists of DNS, Re_τ has been kept moderate for purposes of computational savings and of highlighting the effect of turbulence on flow electrification even at moderate turbulence intensities.

It is worth mentioning that, from the values provided in table II, it can be inferred that the relaxation time of the electric charge ϵ/σ is much larger than the smallest time-scale of turbulent fluctuations ν/u_τ^2. Additionally, given the values of the channel half-width h and Re_τ mentioned above, it can be verified that ϵ/σ is also much larger than the largest time-scale of fluid motion, h/u_b with u_b being the bulk velocity. In other words, the charge-relaxation time is much larger than all relevant hydrodynamic time scales. In turn, this implies that turbulent fluctuations are expected to play a significant role in the redistribution of charges in the flow domain.

It is noted that if the Stern layers are negatively charged, then the diffuse layers and the bulk of the flow are positively charged and vice-versa. In our study, the Stern layers are not resolved because their thickness is at the order of the ion size; instead, for computational purposes, they are assumed to represent the solid-wall boundaries. Then at these boundaries we prescribe the no-slip condition for the velocity and a non-zero Dirichlet condition for the electric charge density ρ_el. In other words, the electric charge in the Stern layers remains constant. Abedian and Sonin [16] justified this choice by observing that, at the interface of an initially uncharged liquid and a solid wall, the charge density at the wall will increase up to an equilibrium value. More specifically, in our simulations the charge density at the boundary is set equal to 10^{-5} C/m^3. Further, a zero-Neumann condition is applied for the electric potential at the top and bottom walls. By virtue of Gauss' law (4), this condition implies that the total charge in the flow domain remains zero. This means that the total charge in the Stern layers is of equal magnitude but opposite sign to the charge in the diffuse layers and in the bulk of the flow.

Initially, we perform a preliminary simulation of turbulent channel flow in absence of electric charge. Once the flow becomes fully developed, we apply the initial profile for the electric charge density and start solving for the coupled system of equations of electrohydrodynamics. In the cross-stream y direction, the initial charge density consists of an exponentially decreasing profile, starting with the (dimensionless) value of unity at the wall and decreasing so that approximately 95% of the initial charge is located within 3 Debye lengths. In this manner, the thickness of the initial charge-density profile corresponds to the actual thickness of the diffuse layer of an EDL[8] for the presumed λ_D. The initial charge-density profile is plotted in figure 2. On the other hand, this profile is constant in the x and z directions.

One may argue that it would be physically more accurate if the initial charge profile was placed in a laminar flow (or in a fluid initially at rest). However, as mentioned above, flow electrification does not occur in the laminar regime unless the Lorentz force is very large. For this reason, we opted to start the simulation with a fully developed turbulent flow profile. This is equivalent to assuming that the amount of charge transported away from the diffuse layers during the laminar-to-turbulent transition period is negligible. This assumption is deemed reasonable since the transition of the flow to the turbulence regime is quite fast.

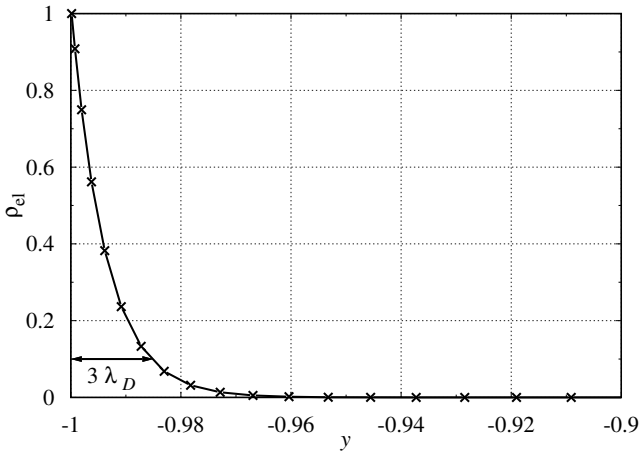

FIG. 2. Initial profile of the charge density along the cross-stream direction for cases A, B and C.

For cases A and B, the computational mesh consists of $192\times128\times128$ grid cells. Whereas for cases C, D and E the mesh consists of $220\times150\times150$ grid cells. The mesh spacing is uniform in the x and z directions. Whereas, in the y direction, the mesh is refined in the near-wall regions in a fashion similar to that of Kim, Moin, and Moser [35]. More specifically, the y coordinates of the edges of the computational cells are given by the general formula,

$$y_j \;=\; h\cos\left(\frac{j-1}{N-1}\pi\right), \qquad j=1,\dots N, \tag{30}$$

where N represents the total number of grid cells in the cross-stream direction; in particular $N=128$ for Cases A and B and $N=150$ for Cases C, D and E. These meshes are sufficiently refined to resolve all essential scales of the flow. A posteriori analysis of the results showed that, for all cases, the ratio of the cell size $(\Delta x\,\Delta y\,\Delta z)^{1/3}$ to the local Kolmogorov scale is not larger than 2 anywhere in the computational domain. Finally, for all the simulations presented therein, we determine the time step via the CFL condition with a constant Courant number set to 0.25.

V. NUMERICAL RESULTS

In this section we present and analyze results from our simulations of cases A-E mentioned in table II. For purposes of non-dimensionalization, the half-width of the channel h is used as the reference length instead of the wall unit because h has the same value in all cases considered herein. Also, the reference time is set equal to the electric relaxation time, $t_\mathrm{el}=\epsilon/\sigma$. The reference charge density is the prescribed value at the walls, ρ_w. All the results presented herein have been made dimensionless with respect to these reference values, with the exception of the fluid velocity which has been non-dimensionalized by the friction velocity u_τ of case C.

Case	Re_τ	k [m^2 s^{-2}]	λ_D [m]	ϵ/σ [s]	D [m^2 s^{-1}]	ν/u_τ^2 [s]
A	150	2.64×10^{-4}	2.50×10^{-5}	18.28	3.42×10^{-11}	1.53×10^{-3}
B	180	3.49×10^{-4}	2.50×10^{-5}	18.28	3.42×10^{-11}	1.06×10^{-3}
C	210	5.30×10^{-4}	2.50×10^{-5}	18.28	3.42×10^{-11}	7.83×10^{-4}
D	210	5.30×10^{-4}	1.77×10^{-5}	9.14	3.42×10^{-11}	7.83×10^{-4}
E	210	5.30×10^{-4}	1.77×10^{-5}	18.28	1.71×10^{-11}	7.83×10^{-4}

TABLE II. Summary of the parameters for the cases considered in our study.

Case	Re_τ	r_t	r_l	Sc
A	150	1.26×10^{-2}	5.00×10^{-3}	2.12×10^{4}
B	180	1.05×10^{-2}	5.00×10^{-3}	2.12×10^{4}
C	210	8.99×10^{-3}	5.00×10^{-3}	2.12×10^{4}
D	210	1.80×10^{-2}	3.53×10^{-3}	2.12×10^{4}
E	210	8.99×10^{-3}	3.53×10^{-3}	4.23×10^{4}

TABLE III. Summary of the dimensionless parameters for the conservation equation of the charge.

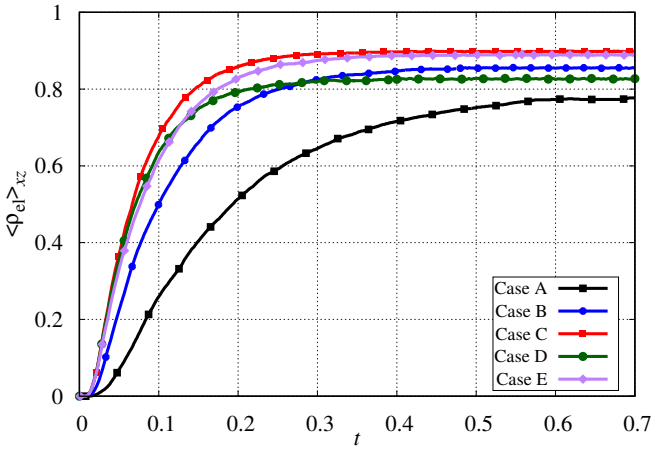

FIG. 3. Time evolution of the area-averaged charge density $\langle\rho_{el}\rangle_{xz}$ at the midplane for the five cases considered herein.

With regard to notation, the time and area average of a generic quantity ψ is denoted by $\langle\psi\rangle$. Whereas, averaging in time only is denoted by $\langle\psi\rangle_t$ and area averaging (at the xz plane) only is denoted by $\langle\psi\rangle_{xz}$. Further, ψ' stands for the fluctuating component of ψ and ψ_{rms} for the root mean square (rms) of ψ', *i.e.* $\psi_{rms} = \langle\psi'\psi'\rangle^{1/2}$. Finally, the turbulent kinetic energy at the midplane k, the values of which are provided in table II, is given by,

$$k = \frac{1}{2}\left(u_{rms}^2 + v_{rms}^2 + w_{rms}^2\right). \tag{31}$$

A. Electrification rate

Our simulations predicted that, for low-conductivity liquids, sufficiently high turbulence intensities do result in flow electrification. This is explained by the fact that as the turbulence intensity increases, the thickness of the hydrodynamic boundary layer decreases. Then, at sufficiently high intensities, it becomes comparable to the thickness of the diffuse layer. In this manner, electric charge is getting entrained in the turbulent structures that are developed in the outer regions of the boundary layer. These structures are subsequently convected by the flow, resulting in the electrification of the liquid in the bulk of the flow.

In our study, the electrification rate is defined as the rate of change of the area-averaged electric charge, $\langle\rho_{el}\rangle_{xz}$, at the midplane of the flow domain. In figure 3 we present plots of the evolution of $\langle\rho_{el}\rangle_{xz}$ at the midplane. These plots help assess the electrification rate for the various cases considered herein, which is simply the slope of the evolution curve of $\langle\rho_{el}\rangle_{xz}$. Globally, we can identify three stages of electrification, regardless of Re_τ and r_t. The first one is characterized by a rapid and almost linear buildup of charge, *i.e.* at a high and almost constant electrification rate. In the second stage the electrification rate decreases, which implies that the ohmic resistance becomes progressively more significant and counteracts the convective transport of charge. In general, the duration of the first stage is approximately half of the duration of the second one. For example, in case C, the first stage terminates at $t \approx 0.1$ while the second one lasts from $t \approx 0.1$ until $t \approx 0.3$. Finally, in the third stage, the charge-density distribution has become statistically stationary. During this stage, the convective transport of charge in the bulk is counterbalanced by the ohmic resistance. Accordingly, the overall charge during the third stage has reached its peak value.

Globally, our simulations predict that both the electrification rate and the amount of charge increase considerably with the turbulence intensity. This is to be expected because, as mentioned above, at higher intensities the thickness of the hydrodynamic layer decreases and, therefore, the number of turbulent structures inside the diffuse layers increases. For example, upon inspection of the slopes of the time evolution of $\langle\rho_{el}\rangle_{xz}$ at the midplane shown in figure 3, we can deduce that in Case C with $Re_\tau = 210$ the electrification rate is almost three times higher than in Case A with $Re_\tau = 150$. Whereas, the required time for the total charge to reach its final value scales in an inverse manner. For instance, in Case A the combined duration of the first two stages is approximately 0.6 time units; by contrast, in Case C it is only 0.3 time units. Also, the final value of $\langle\rho_{el}\rangle_{xz}$ in Case C is approximately 13% higher than that of Case A.

Comparison of the results between cases C and D shows that

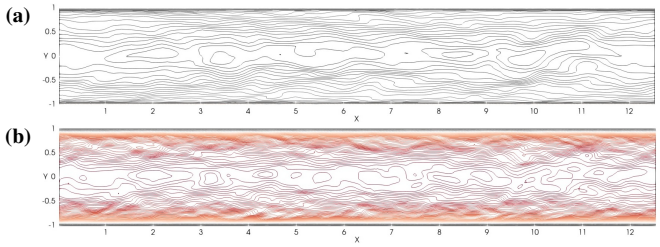

FIG. 4. Case C: instantaneous contour plots of flow variables at an xy-plane during the statistically stationary stage. Each figure contains 100 contours of equally spaced contour-levels. (a) Charge density. (b) Streamwise velocity u.

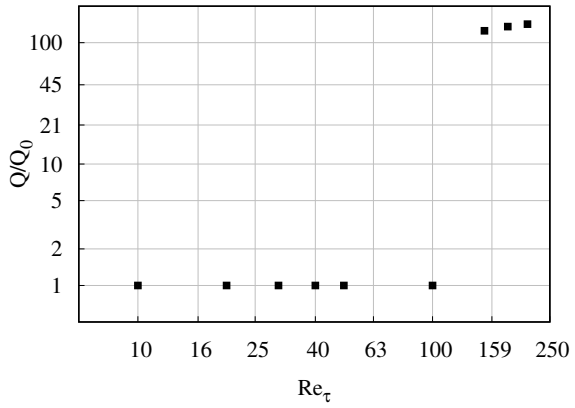

FIG. 5. Variation of the final total charge Q inside the channel with Re_τ. The data in the turbulent regime corresponds to cases A, B and C. Q is non-dimensionalized by the charge in the initial diffuse layers Q_0.

the effect of σ (or, equivalently, r_t) on the electrification rate is rather mild. More specifically, by increasing the conductivity σ hence r_t while keeping all other parameters constant, the electrification rate decreases slightly. On the other hand, r_t has a noticeable effect of the peak (final) value of the electric charge. In particular, according to our simulations, when r_t increases by a factor of 2, the peak (final) value of the midplane charge density, $\langle \rho_{el} \rangle_{xz}$, decreases by approximately 8%. In other words, the material conductivity is an important parameter with regard to the amount of electric charge that will be transported to the bulk of the flow.

Further, by comparing the results for cases C and E we readily infer that the ionic Schmidt number Sc does not affect at all the total amount of charge an has only a very small effect on the electrification rate; when Sc increases, the rate increases slightly too.

In figure 4 we present contour plots of the instantaneous charge density and streamwise velocity component u on the xy plane in the third stage of electrification, *i.e.* when the charge density distribution has become statistically stationary. According to this figure, the contour plots of these two quantities bear certain similarities. For example, steep gradients of both ρ_{el} and u are confined in the near-wall regions but there are also some fluctuations in the bulk of the flow. It is important to add, in all cases considered herein, the magnitude of the Lorentz force is exceedingly small. This, in turn, implies that the electric charge and its redistributions across the flow domain do not have any effect on the fluid motion or the turbulence statistics. This is expected since the prescribed charge density at the walls, ρ_w, has been kept quite small. Evidently, this is a feature of the specific flows under study; for example, in droplet dynamics the coupling between electric field and fluid motion is not negligible[41–43].

Finally in figure 5 we have plotted the value of the final total charge Q inside the channel in terms of the charge in the initial diffuse layers Q_0 and for different Re_τ. We readily observe that for as long as the flow remains laminar, $Re_\tau \lesssim 100$, the charge remains confined in the diffuse layer hence no electrification occurs. However, when the flow becomes turbulent, $Re_\tau \gtrsim 150$, electrification does occur and the amount of charge in the bulk of the flow increases dramatically.

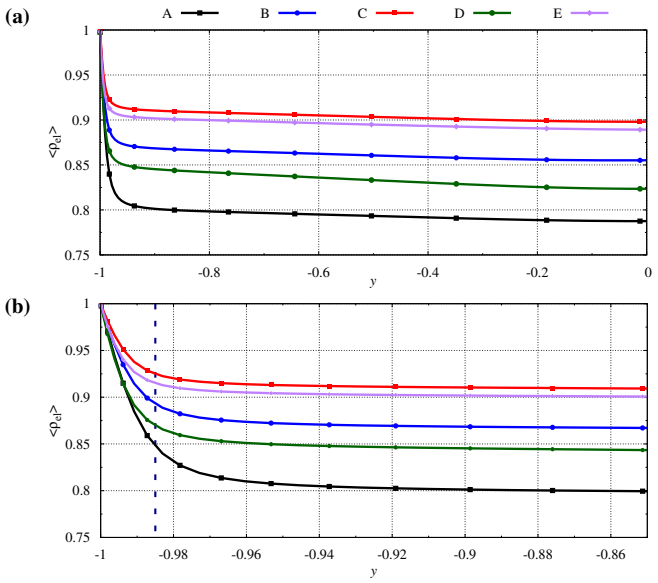

FIG. 6. Profiles of the mean charge density $\langle \rho_{el} \rangle$ for the five cases considered herein. (a) Profiles across the channel. Three distinct zones can be discerned. The thickness δ of the first zone is approximately 0.015 unit lengths, while the thickness of the second zone is approximately 0.15 unit lengths. (b) Zoom of the $\langle \rho_{el} \rangle$ profiles in the first two zones. The vertical dashed line marks, approximately, the end of the first zone and the start of the second one.

B. Charge-density statistics

In this section we present results for the first and second-order statistics of the charge density during the third stage of electrification (during which the charge-density distribution has become statistically stationary). Figure 6a shows profiles of the mean (time and area-averaged) charge density $\langle \rho_{el} \rangle$ along the y axis. In all five cases considered herein, these profiles have the same shape. Further, on the basis of the shapes of the predicted profiles, we can distinguish three different

zones of charge distribution.

The first zone is the one adjacent to the wall and inside both the hydrodynamic boundary layer and the diffuse layer. Inside this zone, the fluid velocity is exceedingly small and the dominant mechanism of transport of charge is via ionic diffusion. As the distance from the wall increases, ohmic resistance convective transport increases while ohmic resistance tends to decrease the charge density. The thickness of this zone, δ, is at the order of 0.015 unit lengths (channel half-widths). From the plots of figure 6a we infer that δ decreases as Re_τ increases. Also, it decreases when σ (or, equivalently, r_t) gets larger. Further, δ increases with the ionic Schmidt number Sc, albeit slightly. As mentioned above, the thickness of the diffuse layer also increases with the Debye length λ_D, which in turn increases with the ionic diffusivity D hence Sc; see, for instance, the results shown in figure 1. In other words, both the first zone and the diffuse layer have the same trend with varying Sc. Actually, the difference between δ and the thickness of the diffuse layer is due to convective currents induced by the velocity fluctuations.

In the second zone, the convective transport of charge becomes important since turbulent eddies displace electric-charge carriers away from the diffuse layer and towards the bulk of the flow. Therefore, the competing mechanisms in this zone are the convective and conductive currents. From figure 3 we infer that, inside this zone, the mean electric charge decreases away from the walls but at a lower rate than in the first one. In the cases examined herein, this zone terminates at approximately 0.15 unit lengths from the wall. Moreover, the thickness of the second zone also decreases as Re_τ or r_t increase, but increases only slightly with Sc. These dependencies are the same as those predicted for the thickness of the first zone δ of the mean-charge distribution. Most noticeably, both the first and second zones become thinner as the turbulence intensity increases.

Finally, the third zone is characterized by a very slow decrease of the charge density away from the walls. Therein, $\langle\rho_{el}\rangle$ and the degree of electrification increase considerably with the turbulence intensity, as expected.

The above observations regarding the thickness of the three zones are corroborated by the rms profiles of the charge density which are presented in figure 7. In these plots, the peaks in the rms values correspond to the end of the first zone (and the start of the second zone). We readily infer that the location of these peaks gets closer to the walls as Re_τ becomes higher.

Additionally, according to the plots of figure 7, the rms values of the charge density across the channel drop with increasing Re_τ; in other words, the fluctuations of ρ_{el} decrease with the turbulence intensity. This is explained by the fact that as turbulence intensity increases, the mixing of electric charge becomes more efficient thereby reducing its fluctuations. The same trend is also observed in passively advected scalars in turbulent flows; for example, in free convection, the rms of the (normalized) temperature decreases as the turbulence becomes more intense[44,45]. In summary, increased turbulence intensities result not only in higher and faster flow electrification but also in less fluctuating charge. Further, according to the plots shown in figure 7, the ohmic resistance has the opposite effect to the charge-density fluctuations. In particular, as the conductivity σ (or, equivalently, r_t) increases, the rms values of ρ_{el} across the channel increase (while its mean values decrease). Finally, it is noted that the ionic Schmidt number has practically no influence on the charge-density fluctuations.

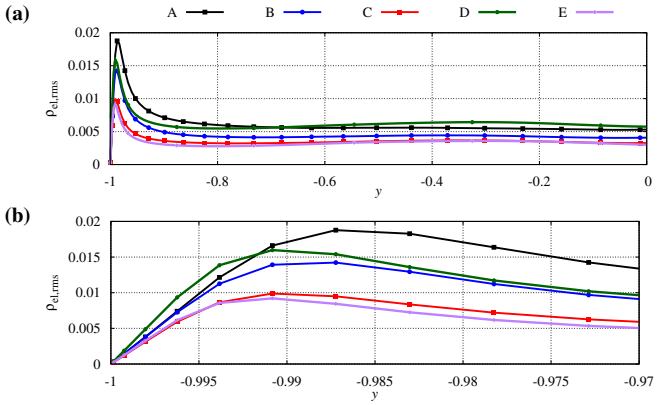

FIG. 7. Rms profiles of the charge density for the five cases considered herein. (a): profile across the channel. (b): zoom of the profiles in the near-wall region.

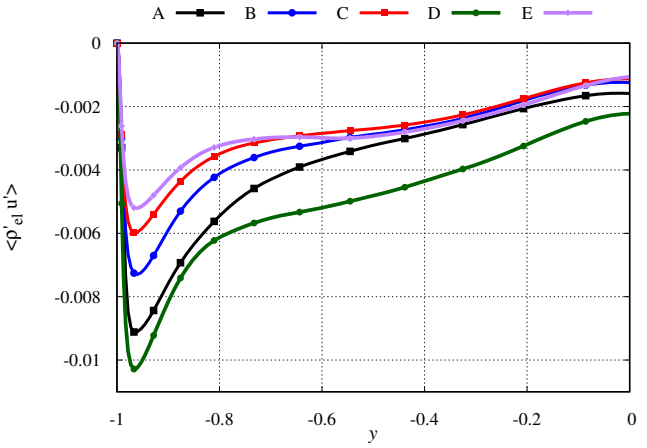

FIG. 8. Profiles of the turbulent charge-density flux $\langle\rho'_{el}u'\rangle$ for the five cases considered in this study.

Similar observations can be drawn for the turbulent charge-density flux $\langle\rho'_{el}u'\rangle$, the profiles of which are presented in figure 8. More specifically, this turbulent flux is suppressed by increasing the turbulence intensity but enhanced considerably by the conductive current. In particular, a twofold rise of σ (or, equivalently, r_t) almost doubles the value of this flux.

Our simulations further predicted that the conductive current affects strongly the flux $\langle\rho'_{el}v'\rangle$ as well. Plots of this quantity are provided in figure 9. From these plots we can infer that, once again, a twofold rise of σ almost doubles the value of $\langle\rho'_{el}v'\rangle$. On the other hand, the effect of the turbulence intensity is much less pronounced and the trend is now reversed: an increase of Re_τ results in a mild increase of this turbulent flux. Further, the peaks of $\langle\rho'_{el}u'\rangle$ profiles are located very close to those of $\rho_{el,rms}$ and its minima are located at the midplane $y = 0$. Whereas, the profiles of $\langle\rho'_{el}v'\rangle$ are

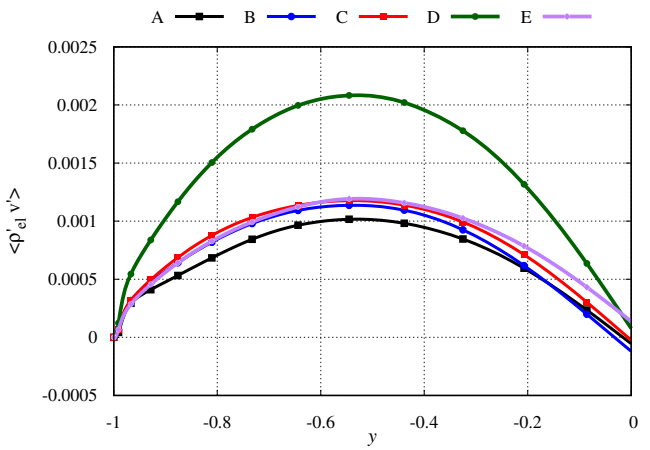

FIG. 9. Profiles of the turbulent charge flux $\langle \rho'_{\rm el} v' \rangle$ for the five cases considered in this study.

anti-symmetric with respect to the midplane and their peaks are located at $y = \mp 0.5$, *i.e.* midway between the channel walls and the midplane. (It can also be inferred from equation (34) below that the antisymmetry of $\langle \rho'_{\rm el} v' \rangle$ is due to the symmetry of $\langle \rho_{\rm el} \rangle$ and its second-order derivative.)

C. Budget of the fluctuating charge-density variance

Below, we derive the equation for the fluctuating charge-density variance (FCV). Further, we elaborate on the FCV budget for the third stage of the electrification process, *i.e.* the statistically stationary stage, and present numerical results of this budget for Case C at $Re_\tau = 210$.

Let $k_{\rm el}$ be defined as $k_{\rm el} = \frac{1}{2}\rho'_{\rm el}\rho'_{\rm el}$. Then $\langle k_{\rm el} \rangle_t$ is one half of the FCV. The procedure for deriving the transport equation for $\langle k_{\rm el} \rangle$ is standard and consists of two steps. In the first one, we multiply every term of (21) with $\rho_{\rm el}$ and then average the result, which yields a transport equation for $\langle \rho_{\rm el}^2 \rangle_t$. In the second step, we take the average of (21) and then multiply the result with $\langle \rho_{\rm el} \rangle_t$, which yields a transport equation for $\langle \rho_{\rm el} \rangle_t^2$. Then, by subtracting the equations derived in these two steps, we obtain the following equation,

$$\underbrace{-\langle \boldsymbol{u} \rangle_t \cdot \nabla \langle k_{\rm el} \rangle_t}_{\mathcal{A}} \underbrace{-\langle \rho'_{\rm el} \boldsymbol{u}' \rangle_t \cdot \nabla \langle \rho_{\rm el} \rangle_t}_{\mathcal{P}} \underbrace{-\langle \boldsymbol{u}' \cdot \nabla k_{\rm el} \rangle_t}_{\mathcal{T}} + \underbrace{D \nabla^2 \langle k_{\rm el} \rangle_t}_{\mathcal{D}}$$
$$\underbrace{-D \langle \nabla \rho'_{\rm el} \cdot \nabla \rho'_{\rm el} \rangle_t}_{\mathcal{E}} \underbrace{-2 \frac{\sigma}{\epsilon} \langle k_{\rm el} \rangle_{xz}}_{\mathcal{F}} = 0. \qquad (32)$$

In the above equation, the terms $\mathcal{A}$, $\mathcal{P}$ and $\mathcal{T}$ describe advection, production and turbulent transport of fluctuating charge-density variance, respectively. The terms $\mathcal{D}$ and $\mathcal{E}$ describe molecular transport and dissipation. Finally, $\mathcal{F}$ is a sink term of FCV due to ohmic resistance.

In the case of channel flow with periodic streamwise and spanwise directions, one can additionally perform area averaging. In this case, the advection term vanishes and the budget

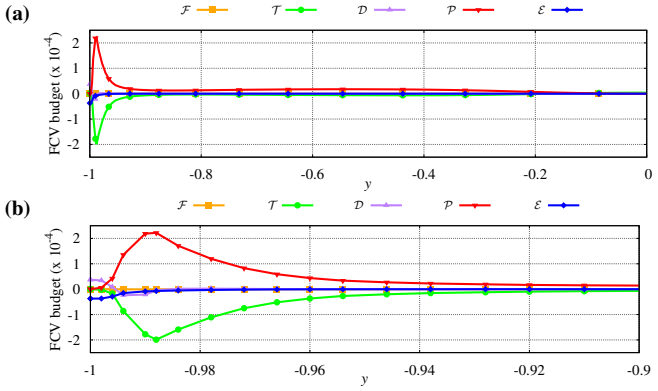

FIG. 10. Budget of the fluctuating charge variance (FCV) at large time for case C. (a): plots across half of the channel. (b): zoom of the plots in the near wall region.

equation (32) assumes the following simplified form,

$$\underbrace{-\langle \rho'_{\rm el} v' \rangle \frac{\mathrm{d}}{\mathrm{d}y} \langle \rho_{\rm el} \rangle}_{\mathcal{P}} \underbrace{-\frac{\mathrm{d}}{\mathrm{d}y} \langle v' k_{\rm el} \rangle}_{\mathcal{T}} + \underbrace{D \frac{\mathrm{d}^2}{\mathrm{d}y^2} \langle k_{\rm el} \rangle}_{\mathcal{D}} \underbrace{-D \langle \nabla \rho'_{\rm el} \cdot \nabla \rho'_{\rm el} \rangle}_{\mathcal{E}}$$
$$\underbrace{-2 \frac{\sigma}{\epsilon} \langle k_{\rm el} \rangle}_{\mathcal{F}} = 0. \qquad (33)$$

In our analysis of the FCV budget, the various terms of this equation were area-averaged (along the periodic x and z directions) and time-averaged over 50 flow-through times during the statistically stationary stage of the electrification process. Upon area and time-averaging, the sum of these terms was smaller than 1.6% of the amplitude of the largest term, which is deemed sufficiently close to zero for the purposes of this study.

Plots of all the terms of (33) are presented in figure 10. According to these plots, adjacent to the wall (first zone of the $\langle \rho_{\rm el} \rangle$ profile), molecular transport $\mathcal{D}$ is counter-balanced by molecular dissipation $\mathcal{E}$, while all other terms practically vanish. On the other hand, inside the second zone, production $\mathcal{P}$ and turbulent transport $\mathcal{T}$ are dominant and balance out one another. The peaks of these terms are located at the edge of the first zone, $y \approx \mp 0.988$. Away from the location of the peaks, both $\mathcal{P}$ and $\mathcal{T}$ decrease substantially in amplitude but are still the dominant terms in the FCV budget. In the third zone, all terms have small amplitude. Nonetheless, $\mathcal{P}$ and $\mathcal{T}$ are still the largest terms and balance each other out. It is worth noting that the amplitude of the term $\mathcal{F}$ related to the conductive currents appears to be negligible in comparison to all other terms across the channel.

D. Mean charge-density profile

Next we consider the mean charge-density equation and derive an approximate solution of it that is close to our numerical predictions. In fact, analytical expressions for the mean

charge-density profiles can provide insight into potential scaling laws for the problem in hand and can also be useful in the development of turbulence models for RANS and LES simulations. The mean charge-density profile for flows in circular pipes has been studied before; see for example Abedian and Sonin [16] as well as the earlier studies[46–48]. Herein we perform an analogous analysis for channel flows.

The equation for the mean charge density is obtained by applying the time and area averaging operator, $\langle\,\rangle$, in (21). For channel flows, the result reads,

$$\frac{\mathrm{d}}{\mathrm{dy}}\langle\rho'_{\mathrm{el}}v'\rangle \;=\; -\frac{\sigma}{\epsilon}\langle\rho_{\mathrm{el}}\rangle + D\frac{\mathrm{d}^2}{\mathrm{dy}^2}\langle\rho_{\mathrm{el}}\rangle\,. \tag{34}$$

The basic idea behind the derivation of a closed-form solution for the mean charge-density is to replace the product $\langle\rho'_{\mathrm{el}}v'\rangle$ in (34) by a gradient term so that the left-hand side becomes a linear elliptic operator. In the context of turbulence modeling, this is referred to as the "gradient-assumption". Let D_{t} denote the turbulent (eddy) diffusivity of the electric charge. Then, $\langle\rho'_{\mathrm{el}}v'\rangle$ is approximated as,

$$\langle\rho'_{\mathrm{el}}v'\rangle \;\approx\; -D_{\mathrm{t}}\frac{\mathrm{d}}{\mathrm{dy}}\langle\rho_{\mathrm{el}}\rangle\,. \tag{35}$$

By introducing (35) into (34) we get

$$-\frac{\sigma}{\epsilon}\langle\rho_{\mathrm{el}}\rangle + (D+D_{\mathrm{t}})\frac{\mathrm{d}^2}{\mathrm{dy}^2}\langle\rho_{\mathrm{el}}\rangle \;=\; 0\,. \tag{36}$$

It can be inferred from figure 9, that this turbulent flux is negligible inside the first zone of the mean charge-density profile. Therefore, D_{t} is much smaller than D therein and can be approximated to zero. Inside the second zone identified above, the turbulent diffusivity increases away from the wall while the gradients of $\langle\rho_{\mathrm{el}}\rangle$ are steep. For the case of pipe flow, Abedian and Sonin [16] assumed that in this region D_{t} increases linearly with the distance from the wall. Herein we make the same assumption and consider a linear profile of D_{t}. Finally, in the third zone, $\langle\rho_{\mathrm{el}}\rangle$ varies very little with respect to y. For this reason, we set therein D_{t} equal to a constant, the value of which is determined by requiring that the resulting mean profile be continuous across the channel and match our numerical results. By applying this procedure, we derive the following parametrization for D_{t},

$$D_{\mathrm{t}} = \begin{cases} 0 & \text{for} \quad 1-\delta < |y| < 1, \\ \dfrac{5}{3}u_\tau(1-|y|) & \text{for} \quad 0.85 \le |y| \le 1-\delta, \\ \dfrac{1}{4}u_\tau & \text{for} \quad |y| \le 0.85, \end{cases} \tag{37}$$

It is interesting to note that according to the proposed model, the only kinematic quantity that affects the mean charge density is the friction velocity.

With this parametrization of D_{t}, the solution of (36) in the first and third zones is given by the same relation as in (29) in which the Debye length λ_{D} is now replaced by $\lambda' = \sqrt{\epsilon(D+D_{\mathrm{t}})/\sigma}$. In the second zone, the solution of (36) is given in terms of modified Bessel functions and reads,

$$\langle\rho_{\mathrm{el}}\rangle = C_1 I_0\left(2\sqrt{\frac{3\sigma}{5\epsilon u_\tau}(1-|y|)}\right) + C_2 K_0\left(2\sqrt{\frac{3\sigma}{5\epsilon u_\tau}(1-|y|)}\right), \tag{38}$$

where I_0 and K_0 are the zeroth-order modified Bessel functions of the first and second kind respectively. Also, C_1 and C_2 are integration constants the values of are computed from the values of $\langle\rho_{\mathrm{el}}\rangle$ at the edges of the second zone.

In figure 11, we present plots of the closed-form profiles of $\langle\rho_{\mathrm{el}}\rangle$, obtained from (36) and (37), for Cases B and C. These plots are juxtaposed with the corresponding results of our DNS. We observe that the closed-form approximate solution agrees reasonably well with the numerical results inside the first zone and the third zone (bulk of the flow). On the other hand, it slightly overestimates the numerical results in the second zone (transition region), which can be attributed to the errors in the presumed form of the eddy diffusivity (37) of D_{t}.

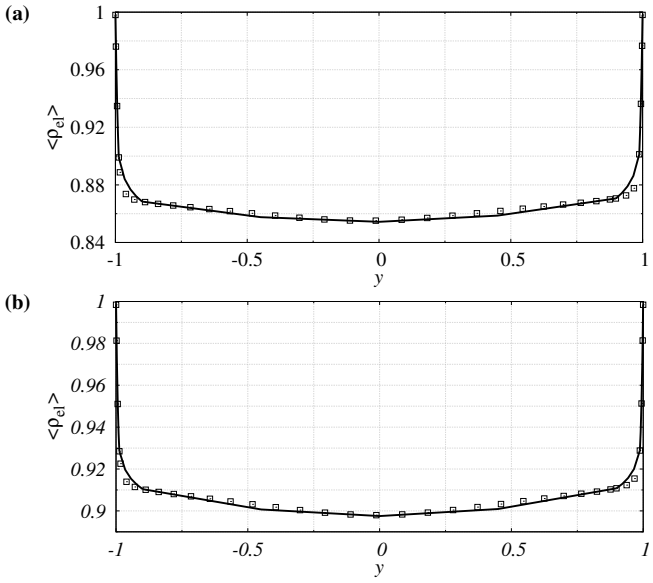

FIG. 11. Plots of the mean charge density $\langle\rho_{\mathrm{el}}\rangle$ along the y axis. (a) Case B. (b) Case C. The black line —— denotes the profiles obtained via numerical simulations, while the squares □ represent the closed-form solution of (36).

VI. CONCLUSIONS

In this paper we have studied electrification in turbulent channel flows of liquid dielectrics via direct numerical simulations. According to our numerical results, the amount of charge transferred to the liquid increases dramatically when the flow becomes turbulent. Also, the electrification rate increases with the turbulence intensity. This is because, as the turbulence intensity increases, the thickness of the hydrodynamic boundary layer becomes comparable to that of the diffuse layer, which enhances the convective transport of charge. Then, electric charge is built up rapidly in the bulk of the flow

until it reaches a plateau and the charge density distribution becomes statistically stationary. In our study the prescribed charge density at the walls was sufficiently small so that the Lorentz force, *i.e.* the volumetric electric force acting on the fluid, was negligible. This in turn implies that the electric field did not affect the fluid motion.

Also, our simulations predicted that, upon electrification, the mean-charge density profile consists of three zones. The first one, is thinner than both the diffuse and hydrodynamic boundary layers and extends up to the peak of the charge-density rms. Inside this zone, electric charge is transported mainly via diffusion. The second zone is the transition region in which convective transport becomes important due to the turbulent motions of the fluid. The third zone extends throughout the bulk of the flow; therein the charge is almost constant. It is also predicted that both the rms and the streamwise turbulent flux of the charge density decrease with the turbulence intensity. On the other hand, the spanwise turbulent flux increases albeit very slightly. Our analysis of the budget of the fluctuating charge-density variance showed that inside the first zone, diffusion and dissipation are dominant and counterbalance one another. Whereas in the second zone, the dominant mechanisms are production and turbulent transport. Finally, we derived an expression for the mean charge-density profile based on the gradient assumption. This profile agrees well with the numerical data for the limited range of Reynolds numbers considered herein. In the future, we plan to perform simulations at higher Reynolds numbers which will allow us to further explore the properties of flow electrification and assess the applicability of the mean profile proposed herein.

ACKNOWLEDGEMENTS

The first and third authors gratefully acknowledge the financial support of the National Research Fund of Belgium (FNRS) under the FLOW-CHARGE grant. The second author gratefully acknowledges the financial support from the European Research Council (ERC) under the European Union's Horizon 2020 research and innovation programme (grant agreement No. 947606 PowFEct).

AUTHORS DECLARATION

The authors have no conflict of interest to disclose.

DATA AVAILABILITY

The data that support the findings of this study are available from the corresponding author upon reasonable request.

[1] P. Atkins, J. de Paula, and J. Keeler, *Atkins' Physical Chemistry*, 11th ed. (Oxford University Press, 2018).
[2] O. Stern, "Zur Theorie der Elektrolytischen Doppelschicht," Z. Elektrochem **30**, 508 (1924).
[3] A. Klinkenberg and J. van der Minne, *Electrostatics in the Petroleum Industry* (Elsevier, 1958).
[4] A. Ohsawa, "Statistical analysis of fires and explosions attributed to static electricity over the last 50 years in japanese industry," J. Phys. Conf. Ser. **301**, 012033 (2011).
[5] G. Touchard, "Streaming currents developed in laminar and turbulent flows through a pipe," J. Electrost. **5**, 463–476 (1978).
[6] G. Touchard, T. W. Patzek, and C. J. Radke, "A physiochemical explanation for flow electrification in low-conductivity liquids in contact with a corronding wall," IEEE Trans Ind Appl. Soc. **32**, 1051–1057 (1996).
[7] G. Domínguez and G. Touchard, "Streaming current development in a rectangular channel," J. Electrost. **40-41**, 153–159 (1997).
[8] T. Paillat, E. Moreau, and G. Touchard, "Space charge density at the wall in the case of heptane flowing through an insulating pipe," J. Electrost. **53**, 171–182 (2001).
[9] J. Cabaleiro, T. Paillat, O. Moreau, and G. Touchard, "Flow electrification of dielectric liquids in insulating channels: limits to the application of the classical wall current expression," J. Electrost. **66**, 79–83 (2008).
[10] H. Krämer, "Kriterien zur Beurteilung der Zündgefahren infolge elektrostatisch aufgeladener Flüssigkeiten." Chem. Ing. Tech. **55**, 419–428 (1983).
[11] J. Cabaleiro, T. Paillat, G. Artana, and G. Touchard, "Flow electrification in turbulent flows of liquids–comparison of two models for one specific case," IEEE Trans. Ind. **55**, 5235–5238 (2019).
[12] G. Touchard, "Turbulent flow electrification with hydrocarbon liquids, liquid hydrogen, liquefied natural gas (LNG) and liquid nitrogen: Part i–three different models," Int. J. Plasma Environ. Sci. **15**, 1–15 (2021).
[13] G. Touchard, "Turbulent flow electrification with hydrocarbon liquids, liquid hydrogen, liquefied natural gas (LNG) and liquid nitrogen: Part II Experiments and comparison with different models," Int. J. Plasma Environ. Sci. **15**, e02012 (2021).
[14] P. Clermont, T. Paillat, Y. Duval, J. Rivenc, and G. Peres, "Flow electrification of an electrically charged liquid," Int. J. Plasma Environ. Sci. Technol. **10**, 125–130 (2016).
[15] P. Clermont, T. Paillat, G. Peres, Y. Duval, and G. Touchard, "Quantification of flow electrification in the context of a tank being filled with a dielectric liquid," IEEE Trans. Ind. Appl. **53 (5)**, 4944–4949 (2017).
[16] B. Abedian and A. Sonin, "Theory for electric charging in turbulent pipe flow," J. Fluid. Mech. **120**, 199–217 (1982).
[17] B. Abedian and A. Sonin, "Electric currents generated by turbulent flows of liquid hydrocarbons in smooth pipes: experiment vs. theory," Chem. Eng. Sci. **41**, 3183–3189 (1986).
[18] B. Hampel and H. Luther, "Effect of impurities on the electrostatic charging of flowing hydrocarbons," Chemie. Ing. Tech. **29**, 323–329 (1957).
[19] A. Ratschow, S. Stein, and H.-J. Gross, "Charge distribution in turbulent flow of charged liquid–modeling and experimental validation," Process Saf. Prog. (2022).
[20] X. Diao, J. Jiang, L. Ni, A. Mebarki, and G. Shen, "Electrification hazard of turbulent pipe flow: Theoretical approach and numerical simulation," Process Saf. Environ. **159**, 84–95 (2022).
[21] J. López-Herrera, S. Popinet, and M. Herrada, "A charge-conservative approach for simulating electrohydrodynamic two-phase flows using volume-of-fluid," J. Comput. Phys. **230**, 1939–1955 (2011).
[22] I. Roghair, D. van den Ende, and F. Mugele, "An OpenFOAM-based electrohydrodynamical model," in *8th Int. Conf. Multiphase Flow* (2013).
[23] M. Calero, H. Grosshans, and M. Papalexandris, "A computational framework for electrification of liquid flows," J. Loss. Prevent. Proc. **74** (2022).
[24] pafiX, `https://www.ptb.de/cms/asep` (2019).
[25] A. Castellanos, "Coulomb-driven convection in electrohydrodynamics," IEEE Trans. Dielectr. Electr. Insul. **26**, 1201–1215 (1991).
[26] D. A. Saville, "Electrohydrodynamics: the Taylor-Melcher leaky dielectric model," Annu. Rev. Fluid Mech. **29**, 27–64 (1997).
[27] A. Castellanos, *Electrohydrodynamics* (Springer-Verlag, 1998).
[28] P. Dumargue, "Perturbations des couches diffuses-I. Equations théoriques de base," Electrochim. Acta **16**, 1115–1128 (1971).
[29] P. Leblanc, J. M. Cabaleiro, T. Paillat, and G. Touchard, "Impact of the laminar flow on the electrical double layer development," J. Electrost. **88**, 76–80 (2017).
[30] T. Paillat, J. Cabaleiro, H. Romat, and G. Touchard, "Flow electrification process: the physicochemical corroding model revisited," IEEE Trans. Dielectr. Electr Insul. **16**, 359–363 (2009).
[31] J. Ferziger and B. Perić, *Computational Methods for Fluid Dynamics*, 4th ed. (Springer-Verlag, 2019).

[32]H. Grosshans, "Modulation of particle dynamics in dilute duct flows by electrostatic charges," Phys. Fluids **30**, 083303 (2018).
[33]H. Grosshans, C. Bissinger, M. Calero, and M. Papalexandris, "The effect of electrostatic charges on particle-laden duct flows," J. Fluid Mech. **909**, A21 (2020).
[34]M. Zeybek and H. Grosshans, "Eulerian formulation for the triboelectric charging of polydisperse powder flows," Phys. Fluids **33**, 063304 (2021).
[35]J. Kim, P. Moin, and R. Moser, "Turbulence statistics in fully developed channel flow at low Reynolds number," J. Fluid. Mech. **177**, 133–166 (1987).
[36]"Chemical book," `https://www.chemicalbook.com/` (2022).
[37]R. Reid, J. Prausnitz, and B. Poling, *The properties of gases and liquids*, 4th ed. (McGraw-Hill, 1987).
[38]A. Brown, P. Levin, and E. Abrahamson, "Dielectric constant of benzene at 25° C by the Wyman method," J. Chem. Phys. **19**, 1226 (1951).
[39]E. O. Forster, "Electric conduction in liquid hydrocarbons. I. Benzene," J. Chem. Phys. **37**, 1021–1028 (1962).
[40]H. Ohshima and K. Furusawa, *Electrical Phenomena at Interfaces : Fundamentals: Measurements, and Applications*, 2nd ed. (CRC Press, 1998).
[41]S. Mandal, A. Bandopadhyay, and S. Chakraborty, "The effect of surface charge convection and shape deformation on the settling velocity of drops in nonuniform electric field," Phys. Fluids **29**, 012101 (2017).
[42]Y. Cui, N. Wang, and H. Liu, "Numerical study of droplet dynamics in a steady electric field using a hybrid lattice boltzmann and finite volume method," Phys. Fluids **31**, 022105 (2019).
[43]Y. Zhang, Z. Su, K. Luo, and H. Yi, "Transient oscillation response characteristics of an electrohydrodynamic settling drop subjected to a uniform electric field," Phys. Fluids **34**, 043601 (2022).
[44]W. Hay and M. Papalexandris, "Numerical simulations of turbulent thermal convection with a free-slip upper boundary," Proc. Roy. Soc. A. **475**, 20190601 (2019).
[45]W. Hay and M. Papalexandris, "Evaporation-driven turbulent convection in water pools," J. Fluid Mech. **904**, A14 (2020).
[46]H. Reichardt, "Vollständige Darstellung der turbulenten Geschwindigkeitsverteilung in glatten Leitungen," Z. Abgew. Math. Mech. **7**, 208–219 (1951).
[47]A. Quarmby and R. Anand, "Non-axisymmetric turbulent mass transfer in a circular tube," J. Fluid Mech. **38**, 447–472 (1969).
[48]B. Petukhov, in *Advances in Heat Transfer, Vol.6*, edited by J. Hartnett and T. Irvine (Academic Press, 1970).